

Atomic-resolution two-dimensional mapping of holes in the cuprate superconductor $\text{La}_{2-x}\text{Sr}_x\text{CuO}_{4\pm\delta}$

Mitsutaka Haruta,^{1,*} Yoshifumi Fujiyoshi,¹ Takashi Nemoto,¹ Akimitsu Ishizuka,² Kazuo Ishizuka,² and Hiroki Kurata¹¹*Institute for Chemical Research, Kyoto University, Uji, Kyoto 611-0011, Japan*²*HREM Research Inc., 14-48 Matsukazedai, Higashimatsuyama, Saitama 355-0055, Japan*

(Received 15 January 2018; published 29 May 2018)

One of the key factors in understanding high- T_c cuprate superconductors is the spatial distribution of holes in the sample. Since x-ray absorption spectroscopy (XAS) and electron-energy-loss spectroscopy (EELS) can directly measure the unoccupied $2p$ states of the oxygen, many experiments have already been performed for a wide range of doping conditions. While polarization-dependent x-ray fluorescence yield absorption cannot spatially resolve different oxygen sites, EELS combined with scanning transmission electron microscopy has the ability to resolve them with atomic resolution. However, since cuprate superconductors are extremely sensitive to electron irradiation, it has not been possible, to date, to characterize them with atomic resolution. Here, we succeeded in atomic-resolution two-dimensional mapping of holes in $\text{La}_{2-x}\text{Sr}_x\text{CuO}_{4\pm\delta}$ by overcoming the problem of irradiation damage using an advanced integration technique. In addition, we have demonstrated the anisotropic chemical bond related to the difference between p_x and p_y orbitals was observed with atomic resolution. The present approach enables atomic-resolution anisotropic spectroscopy and is expected to give information complementary to the polarization-dependent XAS.

DOI: [10.1103/PhysRevB.97.205139](https://doi.org/10.1103/PhysRevB.97.205139)

I. INTRODUCTION

La_2CuO_4 is well known as the parent compound of the high- T_c superconductor of hole-doped type $\text{La}_{2-x}\text{Sr}_x\text{CuO}_4$. With increasing Sr content x , the material property changes from an antiferromagnetic insulator to a superconductor. A maximum T_c occurs at an optimum composition, $x \simeq 0.15$, and then it changes to a normal metal in the overdoped condition [1]. One of the key factors in understanding high- T_c cuprate superconductors is the spatial distribution of holes in the sample. Since x-ray absorption spectroscopy (XAS) and electron-energy-loss spectroscopy (EELS) reflect the unoccupied states, they can directly measure the doped-hole state. Hence, the hole distribution of $\text{La}_{2-x}\text{Sr}_x\text{CuO}_4$ has been investigated for a wide range of doping conditions using Cu L -edge and O K -edge XAS [2–5] and EELS [6]. The studies concluded that the hole is mainly doped into the planar oxygen site in the CuO_2 plane.

However, previous studies could not spatially resolve crystallographically nonequivalent oxygen sites in spite of the importance of their difference. In the first place, while polarization-dependent x-ray fluorescence yield absorption can measure the anisotropy in x , y , and z , it cannot spatially resolve with atomic resolution. On the other hand, EELS combined with scanning transmission electron microscopy (STEM) has the ability to spatially resolve the sites with atomic resolution. Although STEM-EELS analysis has been employed for other cuprate superconductors to study the electronic structure at nonequivalent oxygen sites [7,8], atomic-resolution two-dimensional imaging of holes in oxygen sites

has not been achieved to date because of electron irradiation damage. Electronic state mapping requires spectra with a high signal-to-noise (S/N) ratio from each atomic column in order to resolve the fine structure in O K -edge spectra as well as the individual atomic columns [9–11]. Thus, such a spectrum requires a high total electron dose that often causes irradiation damage even to oxides [10,12]. Unfortunately, advanced low-voltage electron microscopy with a spherical aberration corrector cannot always be employed to overcome this problem. Our preliminary experiment on the present materials revealed that in the case of STEM, the electron damage depends on the electron dose rate (the dose irradiated on one atomic column at a time). This kind of damage is presumably attributable to the loss of oxygen due to the local rise in temperature [13]. Thus, having a low probe current is essential to avoid such damage. However, it is impossible to obtain a spectrum with a high S/N ratio from one atomic column at a low probe current within realistic exposure times owing to the instability of the electron microscope. In the case of conventional spectrum imaging (SI), the amount of the electron dose necessary to obtain a high-S/N-ratio spectrum from one atomic column is higher than the critical dose for many materials. This means that the conventional approach can no longer obtain a high-S/N-ratio spectrum with atomic resolution for such irradiation-sensitive materials. Thus, we need to follow another approach. Here, we succeeded in atomic-resolution two-dimensional mapping of holes in $\text{La}_{2-x}\text{Sr}_x\text{CuO}_{4\pm\delta}$ by overcoming the problem of irradiation damage using an advanced integration technique.

II. METHODOLOGY

The $\text{La}_{2-x}\text{Sr}_x\text{CuO}_{4\pm\delta}$ (LSCO) samples were prepared with a solid-state stoichiometric reaction between La_2O_3 , SrCO_3 ,

*haruta@eels.kuicr.kyoto-u.ac.jp

and CuO. Since preparing overdoped LSCO crystals without oxygen deficiencies was difficult, the amount of excess oxygen δ might not be precise. The crystal structures were confirmed with x-ray diffraction [14].

STEM-EELS was carried out at room temperature on a JEM-ARM200F equipped with a monochromator and an electron-energy-loss spectrometer (Gatan, Inc., GIF Quantum ERS). The experiments were performed at 200 kV owing to the electron irradiation problem (see the Supplemental Material [15]). The convergent semiangle of the incident electron probe was 24.6 mrad. The inner and outer angles of the annular detector were 57.3 and 114.6 mrad, respectively, and the EELS collection semiangle was 57.3 mrad. The specimens were observed along the [100] zone axis. The practical energy resolution for monochromated O K -edge spectra obtained using an energy dispersion of 0.05 eV/pixel was 0.25 eV, while that for the atomic-resolution nonmonochromated spectra obtained using a 0.25 eV/pixel energy dispersion was 1.25 eV. The $\text{La}_{2-x}\text{Sr}_x\text{CuO}_{4\pm\delta}$ series has a very low resistance to electron irradiation [13], with doped samples being particularly prone to damage. In order to achieve atomic-resolution imaging without specimen damage, a low probe current (21 pA) and a short dwell time of 5 ms were used with a scan step of 0.651 nm/pixel. SI data were acquired from a $32.55 \times 130.2 \text{ nm}^2$ ($50 \times 200 \text{ pixel}^2$) region. The total acquisition time for a single SI data point was 66 s. The total dose for single SI was $2.4 \times 10^3 \text{ C/cm}^2$. Such experimental conditions were the practical limit, maintaining atomic resolution without causing irradiation damage. This is a very low dose condition compared with previous results for the O K edge of cuprate superconductors [7,8] and the C K edge of graphene [16].

Figure 1(a) show the high-angle annular dark-field (HAADF) STEM image of $\text{La}_{1.85}\text{Sr}_{0.15}\text{CuO}_{4\pm\delta}$ along the [100] direction taken over 50×200 points under the same conditions as the present experiments. La (Sr) and Cu atomic columns were easily observed with z contrast. The distortion of the image due to the instability was relatively small because of the vertically long acquisition region, which was advantageous to the postprocess. The SI measurements were carried out using dual EELS. Each spectrum shifted slightly during the SI measurement using prism shift. The high-quality dark reference was removed from the raw SI data [17]. Then the zero-loss peak was aligned, and the measured peak shifts were applied to sibling core-loss SI to reduce the gain variation of the CCD [17–19]. The S/N ratio of the total spectrum [Fig. 1(c)] was very high thanks to the summation and reduction of noise, although the individual single spectrum was very noisy, as seen in Fig. 1(b), where the count of the single spectrum is comparable to the dark count in the gain-normalized mode.

After many atomic-resolution SI data were obtained, we selected a subset of these data according to the following two criteria: (i) a relative thickness (t/λ) of less than 0.7 and (ii) no damage in the total spectrum of SI (the sum of 10000 spectra) compared with the spatially averaged O K -edge spectrum [Fig. 1(d)] which was measured with a large scan step and the defocusing condition to obtain the spectrum of the bulk without damage. In comparison to the spatially averaged spectrum [Fig. 1(d)], the present conditions [Fig. 1(e)] allowed both the atomic-resolution images and the spectra to be taken and several measurements to be made in the same region without

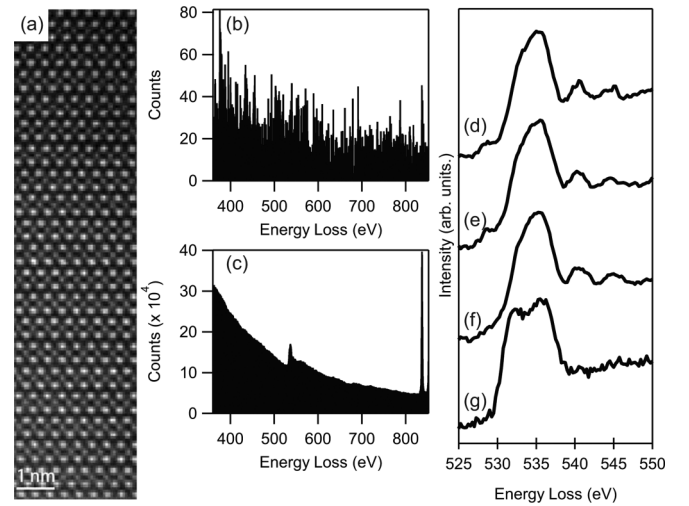


FIG. 1. (a) HAADF-STEM image ($50 \times 200 \text{ pixels}$) of $\text{La}_{1.85}\text{Sr}_{0.15}\text{CuO}_{4\pm\delta}$ along the [100] zone axis of the SI area under 200 kV. The scan step was 0.651 nm/pixel, and dwell time was 5 ms/pixel. (b) A single spectrum and (c) the sum of 10,000 spectra in SI. The differences in bulk O K -edge spectra are due to differences in experimental conditions: (d) probe current $I_p = 70 \text{ pA}$, scan step = 1 nm/pixel, dwell time = 20 ms/pixel, defocused conditions; (e) $I_p = 21 \text{ pA}$, scan step = 0.651 nm/pixel, dwell time = 5 ms/pixel; (f) $I_p = 21 \text{ pA}$, scan step = 0.651 nm/pixel, dwell time = 10 ms/pixel; and (g) heavy-damage conditions. All spectra are the sum of 10,000 spectra with individual conditions.

any damage. On the other hand, even a slight increase in dwell time from 5 to 10 ms (with all other conditions being the same) causes the prepeak (528.5 eV) to disappear owing to irradiation damage, as shown in Fig. 1(f). This damage cannot be detected in the HAADF-STEM image. In addition, under a higher dose rate, the fine structure of the O K edge changes, as shown in Fig. 1(g).

If the many crystallographically equivalent positions could be integrated at a specific point, we might be able to realize atomic-resolution spectroscopy from the data acquired under the present conditions. However, the atomic-scale HAADF-STEM image obtained in the SI mode is distorted due to the long acquisition time for the core-loss spectrum in almost every case. Therefore, it is difficult to correct the specimen drift for multiple HAADF images using rigid registration because of the variety of image distortion depending on the instability of the electron microscope. Recently, Jones *et al.* reported that nonrigid registration is very effective in reducing image drift and improving the S/N ratio [20,21]. In addition to adopting this technique, in the present study, we evolved this integration technique by combining it with a template-matching technique. Since the aim of this research was to distinguish the inequivalent oxygen site within a unit cell, we devised the following procedure. First, we obtained many SI data with atomic resolution from a wide single-crystal region using a low-current condition. Next, we obtained a nondistorted HAADF image with the same scan step using a fast dwell time, and it was defined as the template image. The size of the template image was comparable to the unit cell. Then, we selected many crystallographically equivalent

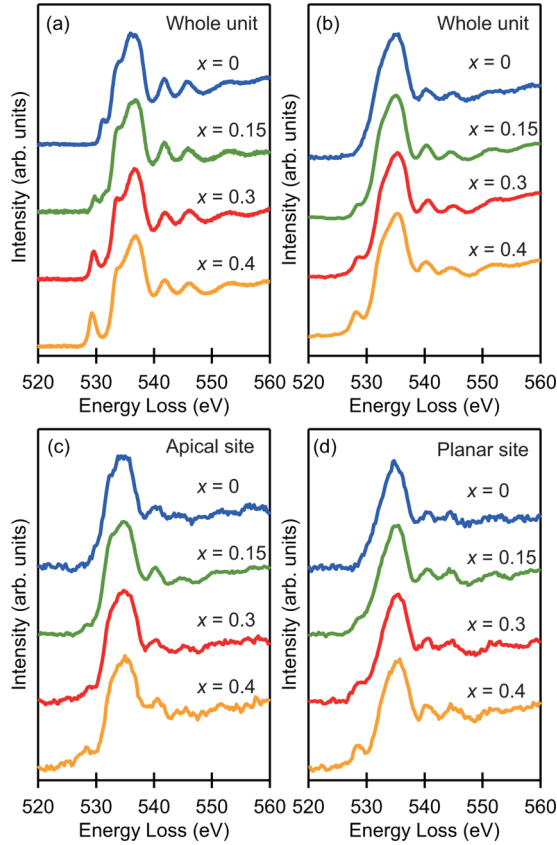


FIG. 2. O K -edge spectra of $\text{La}_{2-x}\text{Sr}_x\text{CuO}_{4\pm\delta}$. (a) Monochromated spectra (0.05 eV/pixel) averaged over the whole unit, (b) atomic-resolution spectra (0.25 eV/pixel) averaged over the whole unit, and (c) apical and (d) planar oxygen site spectra after nonrigid alignment (0.25 eV/pixel).

regions from a target HAADF-STEM image by judging the correlation with the template image (template matching) and applied rigid and nonrigid registration of these equivalent regions to fit the template image and finally applied them to the corresponding SI data by using the SMARTALIGN software package (HREM Research). Upon repeating this procedure over many SI data, the S/N ratio improved dramatically thanks to the increase in the signal by accumulation and the decrease in the noise by gain averaging, maintaining spatial resolution without causing irradiation damage. The total accumulation numbers of the spectra including rotation symmetry were 12 008, 14 348, and 4712 for the $x = 0.15$, 0.3, and 0.4 samples, respectively.

III. RESULTS AND DISCUSSION

Figure 2(a) shows monochromated O K -edge spectra (0.05 eV/pixel) averaged over the whole unit cell. The prepeak (528.5 eV) that appears for doped samples corresponds to holes (Zhang-Rice singlet) in the oxygen $2p$ state, and that (531 eV) for the nondoped sample corresponds to the unoccupied oxygen $2p$ state hybridized with the upper Hubbard band of the Cu $3d$ state [$b_{1g}(d_{x^2-y^2})$ state owing to the Jahn-Teller effect]. As previously reported [2–6], the hole peak intensifies with increasing Sr content. In the case of our atomically

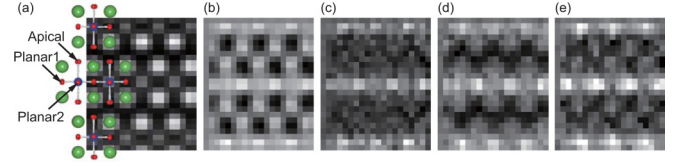


FIG. 3. Atomic-resolution hole mapping. (a) Template HAADF image of $\text{La}_{2-x}\text{Sr}_x\text{CuO}_{4\pm\delta}$ observed along the [100] zone axis of the tetragonal phase. La (Sr), Cu, and O atoms correspond to green, blue, and red, respectively. (b) Atomic-resolution oxygen mapping of $\text{La}_{1.85}\text{Sr}_{0.15}\text{CuO}_{4\pm\delta}$. Atomic-resolution hole mapping of (c) $x = 0.15$, (d) $x = 0.3$, and (e) $x = 0.4$.

resolved experiment, we used a low dispersion (0.25 eV/pixel) because of the weak signal intensity resulting from the low dose. Nevertheless, an increase in hole peak intensity is still observed, as shown in Fig. 2(b). Figures 2(c) and 2(d) show the spectra for the center of the apical and purely planar oxygen sites [labeled planar1 in Fig. 3(a)], respectively.

Figure 3 shows the results obtained by template matching and nonrigid registration. Figure 3(a) shows an atomic-resolution HAADF-STEM image observed along the [100] zone axis. In $\text{La}_{2-x}\text{Sr}_x\text{CuO}_{4\pm\delta}$, the CuO_6 octahedrons are extended along the c axis due to the Jahn-Teller effect of the Cu^{2+} ion. As a result, there are two crystallographically inequivalent oxygen sites: the apical O in the LaO layers and the planar O in the CuO_2 layers. In addition, there are two types of planar O atomic columns, labeled planar1 and planar2 in Fig. 3(a). Figure 3(b) shows atomic-resolution oxygen mapping of $\text{La}_{1.85}\text{Sr}_{0.15}\text{CuO}_{4\pm\delta}$, where a 50 eV energy window from the threshold was used. The O mapping shows comparable contrasts for both oxygen sites. Figures 3(c)–3(e) show atomic-resolution hole maps obtained using hole-peak signals (1.5 eV window) of the O K edge with $x = 0.15$, 0.3, and 0.4, respectively. In the case of $x = 0.15$, the hole map exhibits an anisotropic distribution, where only the planar oxygen sites are displayed brightly. On the other hand, in the case of the overdoped samples ($x = 0.3$ and 0.4), apical oxygen sites increase in brightness. The spectrum extracted from the center of the apical oxygen site in the $x = 0.15$ sample [Fig. 2(c)] looks like a very weak prepeak. Given that energy-selected mapping using the integrated intensity of a specific peak reflects the excitation probability of a particular energy loss at a specific position, the weak intensity of the prepeak is considered to be attributable to the excitation of the neighbor planar site due to the delocalization of inelastic electron and dechanneling effects. If the origin of the peak is the planar site, the two-dimensional mapping should show a local maximum at its site. On the other hand, previous results of polarization-dependent fluorescence yield absorption have shown a small chemical shift between the prepeaks in spectra measured under $E_h \perp c$ and $E_h \parallel c$ conditions [2]. The present results also indicated a small chemical shift between the prepeaks of apical and planar oxygen sites. Thus, we conclude that the prepeak observed at the apical oxygen site in the $x = 0.15$ case cannot be attributed to the mixing of planar sites, but rather is due to the intrinsic peak of the apical oxygen site. Although such very weak intensities have been difficult to observe on a two-dimensional map due to the

comparable intensity of noise in such a low-dose condition, our results demonstrate the different hole distributions obtained in under- and overdoped conditions and directly provide the spatial distribution of holes in cuprate superconductors.

Next, we consider the hole maps [Figs. 3(c)–3(e)] in detail, where planar 2 oxygen columns appear darker than planar 1 oxygen columns. Surprisingly, since this contrast difference is larger than that in the oxygen elemental mapping, which represents the so-called dynamical effect [Fig. 3(b)] [22], the fact that the planar 2 oxygen columns appear darker can be attributed to the anisotropy of the chemical bonds between Cu and O atoms in the CuO_2 plane. It is thought that since the hole-state orbital ($2p_x$ or $2p_y$) of planar O points toward Cu, the intensity of the prepeak is affected by the orbital orientation with respect to the direction of momentum transfer upon inelastic scattering. In our STEM-EELS experiment, however, the momentum transfer was mainly in the plane perpendicular to the electron direction. If, as in the planar 1 oxygen columns, the hole state ($2p_x$) in planar oxygen is perpendicular to the electron beam, the prepeak intensity must be higher than that ($2p_y$) at the CuO column. The anisotropy of oxygen bonding in the fine structure of atomic-resolution EELS has been reported previously for SrTiO_3 [23]. In that study, however, the spectral change due to the anisotropy in the atomic sites was not detected in the raw data, but rather emerged only after an inversion process which could remove the mixing of signals. By contrast, we were able to observe the difference directly on the two-dimensional map, owing to the dramatic improvement in the S/N ratio of the atomic-scale spectrum. Therefore, the present approach demonstrates an atomic-resolution anisotropic spectroscopy and is expected to give complementary information to the polarization-dependent XAS.

Figure 4 shows the prepeak intensity as a function of Sr concentration x . The spectrum intensities were normalized at the main peak, and the prepeak intensities were obtained by integrating a single Gaussian fitted to the spectrum. Looking at the profile for the bulk, the intensity does not increase linearly with x . This can be explained by the fact that, under overdoped conditions, the holes also occupy the Cu d orbitals [24]. As described above, not only the absolute intensity of the prepeak but also the relative intensity of the main peak varies with position in planar oxygen sites. Thus, for a quantitative comparison of the intensities of purely apical and planar oxygen columns, we must take into account the direction of the chemical bonds. The ratios of the prepeak intensities of the apical oxygen sites to those of the planar oxygen sites were 44.4%, 73.1%, and 78.0% for the $x = 0.15$, 0.3, and 0.4 samples, respectively. Although these values may contain a mixing component due to the delocalization of inelastic

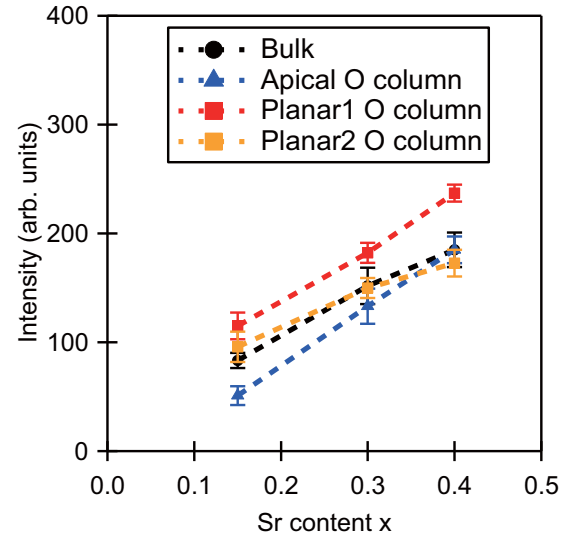


FIG. 4. Quantitative comparison of the intensities of the prepeak. The intensity of the state of holes on O sites as a function of Sr content x . Dashed lines are merely guides to the eye. The error bars are the standard deviation σ of observed oxygen columns.

scattering, we believe that the mixing is insignificant. The results confirm that under overdoped conditions, the doped holes mostly enter apical, rather than planar, oxygen sites.

IV. SUMMARY AND CONCLUSIONS

We have demonstrated atomic-resolution two-dimensional hole mapping by using evolved nonrigid registration combined with a template-matching technique for thousands of spectra. We found that improving the S/N ratio allowed us to characterize the anisotropy in the chemical bonds with atomic resolution, associated with the difference in orientation between oxygen p_x and p_y . As a consequence, we obtained a quantitative comparison of hole concentration between apical and planar sites. The present approach is applicable to not only many other radiation-sensitive materials but also an interface region whose structure is equivalent along the in-plane direction by changing the size of the template image.

ACKNOWLEDGMENTS

This work was supported by JSPS KAKENHI (Grants No. 26706015 and No. 17H02739) and partly supported by JSPS Core-to-Core Program (A) Advanced Research Networks. The assistance of Dr. Kimoto, Dr. Nagai, and Dr. Nagao with sample synthesis is gratefully acknowledged.

- [1] J. B. Torrance, Y. Tokura, A. I. Nazzari, A. Bezing, T. C. Huang, and S. S. P. Parkin, *Phys. Rev. Lett.* **61**, 1127 (1988).
- [2] C. T. Chen, L. H. Tjeng, J. Kwo, H. L. Kao, P. Rudolf, F. Sette, and R. M. Fleming, *Phys. Rev. Lett.* **68**, 2543 (1992).
- [3] C. T. Chen, F. Sette, Y. Ma, M. S. Hybertsen, E. B. Stechel, W. M. C. Foulkes, M. Schluter, S.-W. Cheong, A. S. Cooper,

L. W. Rupp, Jr., B. Batlogg, Y. L. Soo, Z. H. Ming, A. Krol, and Y. H. Kao, *Phys. Rev. Lett.* **66**, 104 (1991).

- [4] E. Pellegrin, N. Nücker, J. Fink, S. L. Molodtsov, A. Gutiérrez, E. Navas, O. Strebel, Z. Hu, M. Domke, G. Kaindl, S. Uchida, Y. Nakamura, J. Markl, M. Klauda, G. Saemann-Ischenko, A. Krol, J. L. Peng, Z. Y. Li, and R. L. Greene, *Phys. Rev. B* **47**, 3354 (1993).

- [5] N. B. Brookes, G. Ghiringhelli, A. M. Charvet, A. Fujimori, T. Kakeshita, H. Eisaki, S. Uchida, and T. Mizokawa, *Phys. Rev. Lett.* **115**, 027002 (2015).
- [6] H. Romberg, M. Alexander, N. Nücker, P. Adelman, and J. Fink, *Phys. Rev. B* **42**, 8768 (1990).
- [7] N. Gauquelin, D. G. Hawthorn, G. A. Sawatzky, R. X. Liang, D. A. Bonn, W. N. Hardy, and G. A. Botton, *Nat. Commun.* **5**, 4275 (2014).
- [8] M. Bugnet, S. Löffler, D. Hawthorn, H. A. Dabkowska, G. M. Luke, P. Schattschneider, G. A. Sawatzky, G. Radtke, and G. A. Botton, *Sci. Adv.* **2**, e1501652 (2016).
- [9] M. Haruta, K. Kurashima, T. Nagai, H. Komatsu, Y. Shimakawa, H. Kurata, and K. Kimoto, *Appl. Phys. Lett.* **100**, 163107 (2012).
- [10] M. Haruta, T. Nagai, N. R. Lugg, M. J. Neish, M. Nagao, K. Kurashima, L. J. Allen, T. Mizoguchi, and K. Kimoto, *J. Appl. Phys.* **114**, 083712 (2013).
- [11] H. Tan, S. Turner, E. Yücelen, J. Verbeeck, and G. Van Tendeloo, *Phys. Rev. Lett.* **107**, 107602 (2011).
- [12] G. A. Botton, S. Lazar, and C. Dwyer, *Ultramicroscopy* **110**, 926 (2010).
- [13] M. Gao, L. M. Peng, X. L. Dong, B. R. Zhao, G. D. Liu, and Z. X. Zhao, *Phys. Rev. B* **62**, 5413 (2000).
- [14] P. G. Radaelli, D. G. Hinks, A. W. Mitchell, B. A. Hunter, J. L. Wagner, B. Dabrowski, K. G. Vandervoort, H. K. Viswanathan, and J. D. Jorgensen, *Phys. Rev. B* **49**, 4163 (1994).
- [15] See Supplemental Material at <http://link.aps.org/supplemental/10.1103/PhysRevB.97.205139> for the effect of low-voltage microscopy on $\text{La}_{2-x}\text{Sr}_x\text{CuO}_{4\pm\delta}$.
- [16] K. Suenaga and M. Koshino, *Nature (London)* **468**, 1088 (2010).
- [17] V.-D. Hou, *Microsc. Microanal.* **15**, 226 (2009).
- [18] Y. Sasano and S. Muto, *J. Electron Microsc.* **57**, 149 (2008).
- [19] M. Bosman and V. J. Keast, *Ultramicroscopy* **108**, 837 (2008).
- [20] L. Jones, H. Yang, T. J. Pennycook, M. S. J. Marshall, S. Van Aert, N. D. Browning, M. R. Castell, and P. D. Nellist, *Adv. Struct. Chem. Imaging* **1**, 8 (2015).
- [21] S. Wenner, L. Jones, C. D. Marioara, and R. Holmestad, *Micron* **96**, 103 (2017).
- [22] M. Bosman, V. J. Keast, J. L. García-Muñoz, A. J. D'Alfonso, S. D. Findlay, and L. J. Allen, *Phys. Rev. Lett.* **99**, 086102 (2007).
- [23] M. J. Neish, N. R. Lugg, S. D. Findlay, M. Haruta, K. Kimoto, and L. J. Allen, *Phys. Rev. B* **88**, 115120 (2013).
- [24] Y. Sakurai, M. Itou, B. Barbiellini, P. E. Mijnders, R. S. Markiewicz, S. Kaprzyk, J.-M. Gillet, S. Wakimoto, M. Fujita, S. Basak, Y. J. Wang, W. Al-Sawai, H. Lin, A. Bansil, and K. Yamada, *Science* **332**, 698 (2011).